Inorganic Chemistry

Article

pubs.acs.org/IC

Lanthanide Metalloligand Strategy toward d–f Heterometallic Metal–Organic Frameworks: Magnetism and Symmetric-Dependent Luminescent Properties

Xiao-feng Huang,[†] Jing-xin Ma,[‡] and Wei-sheng Liu*[,†]

[†]Key Laboratory of Nonferrous Metal Chemistry and Resources Utilization of Gansu Province and State Key Laboratory of Applied Organic Chemistry, Lanzhou University, Lanzhou 730000, P. R. China

[‡]College of Chemistry and Chemical Engineering, Ningxia University, Yinchuan 750021, P. R. China

Supporting Information

ABSTRACT: On the basis of lanthanide metalloligands, $[Ln(ODA)_3]^{3-}$ (H_2ODA = oxydiacetic acid), three series of d–f heterometallic metal–organic frameworks, $\{[Co(H_2O)_6]\cdot[Ln_2(ODA)_6Co_2]\cdot 6H_2O\}_n$ [**1**; Ln = Gd (**1a**), Dy (**1b**), and Er (**1c**)], $\{[Ln_2(ODA)_6Cd_3(H_2O)_6]\cdot mH_2O\}_n$ [**2**; Ln = Pr (**2a**), Nd (**2b**), Sm (**2c**), Eu (**2d**), and Dy (**2e**), m = 9, 6, or 3], and $\{[Cd(H_2O)_6]\cdot[Ln_2(ODA)_6Cd_2]\cdot mH_2O\}_n$ [**3**; Ln = Dy (**3a**), Ho (**3b**), Er (**3c**), Tm (**3d**), and Lu (**3e**), m = 6 or 12], were designed and synthesized by a solvent volatilization and hydrothermal method. Magnetic investigation of **1** reveals the ferromagnetic interactions between the metal ions. In **2**, Ln^{III} ions occupied the inversion centers, which are confirmed by the fact that the emission intensity ratio of $^5D_0 \rightarrow {}^7F_1$ to $^5D_0 \rightarrow {}^7F_2$ of the Eu^{III} ion is much more than 3 in **2d**. It is worth noting that, in **2d**, the intensity ratio $I(^5D_0 \rightarrow {}^7F_1)/I(^5D_0 \rightarrow {}^7F_2)$ could decrease significantly upon the introduction of different hydrophilic guest molecules, which implies that the luminescent properties of **2d** have a strong dependence on the geometry of the first coordination sphere of the Eu^{III} ion.

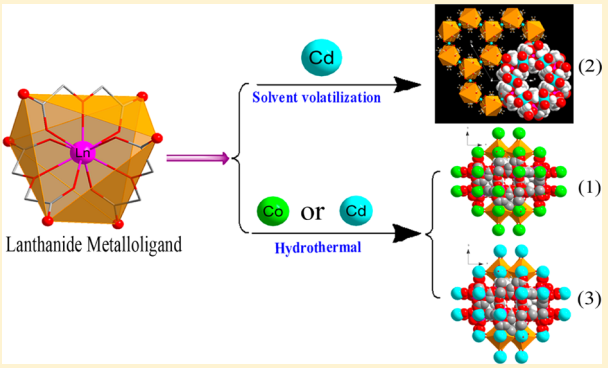

1. INTRODUCTION

Over the past decade, the rational design and construction of d–f heterometallic metal–organic frameworks (HMOFs) have provoked the interest of chemists because of their potential applications in the fields of magnetism, luminescence, ion exchange, gas adsorption, and bimetallic catalysis, as well as their impressive structural diversity in terms of architecture and topology.[1] Up to now, several different synthetic methodologies have been employed to fabricate d–f HMOFs.[2] Among the reported strategies, the metalloligand strategy is an effective way to construct functional HMOFs.[3] However, compared with d-block metalloligands, f-block metalloligands, especially lanthanide metalloligands, were very rare.[4] However, lanthanide ions are well-known candidates for displaying enhanced photoluminescent properties attributing to f–f transitions. This is especially true for Eu^{III} and Tb^{III} complexes. So, if luminescent metalloligands were obtained, the luminescent HMOFs could be constructed.[5] Furthermore, because of the magnitude of the spin, as well as the spin–orbit-coupling-based magnetic anisotropy that 4f species display, lanthanide metalloligands should display enhanced magnetic properties, which could be used to assemble magnetic HMOFs.[6] At the same time, transition-metal (TM) ions, such as Co^{II} and Cd^{II}, exhibit peculiar physical properties especially magnetism and luminescence by virtue of diverse d electrons. Thus, the combination of lanthanide metalloligands and TM ions in one metal–organic framework could provide an avenue for the construction of novel magnetic or luminescent materials.

In a previous work, we demonstrated the one example of rare Cd–Ln HMOFs constructed by lanthanide metalloligand, $[Ln(ODA)_3]^{3-}$ (H_2ODA = oxydiacetic acid).[4c] Inspired by this work, we wondered whether the lanthanide metalloligand would construct other 3d–4f and/or 4d–4f HMOFs to open a new way to functional materials, and as a result, we still used $[Ln(ODA)_3]^{3-}$ as the metalloligand to assemble three series of d–f HMOFs, $\{[Co(H_2O)_6]\cdot[Ln_2(ODA)_6Co_2]\cdot 6H_2O\}_n$ [**1**; Ln = Gd (**1a**), Dy (**1b**), and Er (**1c**)], $\{[Ln_2(ODA)_6Cd_3(H_2O)_6]\cdot mH_2O\}_n$ [**2**; Ln = Pr (**2a**), Nd (**2b**), Sm (**2c**), Eu (**2d**), and Dy (**2e**)], and $\{[Cd(H_2O)_6]\cdot[Ln_2(ODA)_6Cd_2]\cdot mH_2O\}_n$ (**3**) [Ln = Dy (**3a**), Ho (**3b**), Er (**3c**), Tm (**3d**), and Lu (**3e**)] under different synthesis approaches (Scheme 1).

In addition, the magnetism of complex **1** and the guest-induced luminescence of **2d** were investigated.

2. EXPERIMENTAL SECTION

Caution! *Perchlorate salts of metal complexes with organic ligands are potentially explosive. Only small amounts of material should be prepared,*

Received: December 16, 2013
Published: June 2, 2014

   dx.doi.org/10.1021/ic403080n | Inorg. Chem. 2014, 53, 5922–5930

Scheme 1. Lanthanide Metalloligand and Synthesis Methods of Complexes 1−3

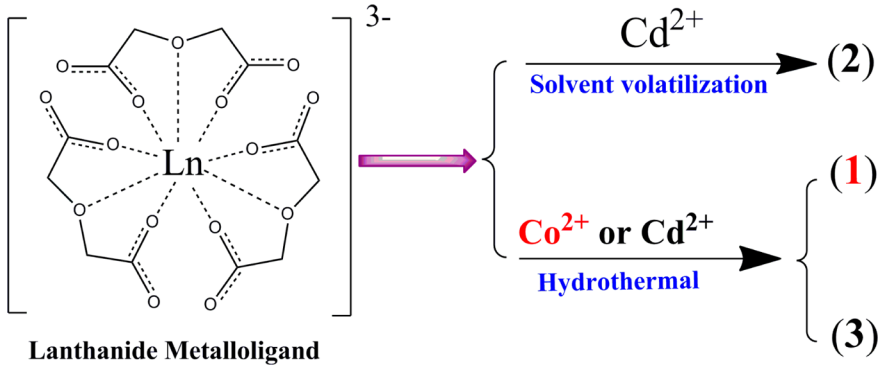

Table 1. Crystal Data and Structural Refinement Parameters for 1−3

	1a	1b	1c	2a	2b	2c
formula	$C_{24}H_{48}Gd_2Co_3O_{42}$	$C_{24}H_{48}Dy_2Co_3O_{42}$	$C_{24}H_{48}Er_2Co_3O_{42}$	$C_{24}H_{54}Pr_2Cd_3O_{45}$	$C_{24}H_{48}Nd_2Cd_3O_{42}$	$C_{24}H_{48}Sm_2Cd_3O_{42}$
M_r	1499.91	1510.41	1519.93	1681.71	1634.33	1646.57
T (K)	296(2)	296(2)	296(2)	298(2)	298(2)	298(2)
cryst syst	cubic	cubic	cubic	hexagonal	hexagonal	hexagonal
space group	$Fd\bar{3}c$	$Fd\bar{3}c$	$Fd\bar{3}c$	$P6/mcc$	$P6/mcc$	$P6/mcc$
a (Å)	25.7619(4)	25.6617(5)	25.5382(8)	12.9706(8)	12.7559(18)	12.8326(11)
b (Å)	25.7619(4)	25.6617(5)	25.5382(8)	12.9706(8)	12.7559(18)	12.8326(11)
c (Å)	25.7619(4)	25.6617(5)	25.5382(8)	17.615(2)	17.741(2)	17.756(2)
α (deg)	90	90	90	90	90	90
β (deg)	90	90	90	90	90	90
γ (deg)	90	90	90	120	120	120
V (Å^3)	17097.5(8)	16898.8(10)	16656.0(16)	2566.4(4)	2499.9(6)	2532.3(4)
Z	16	16	16	2	2	2
D_{calcd} (mg/cm^3)	2.153	2.346	2.396	2.321	2.171	2.159
μ (mm^{-1})	4.314	4.780	5.292	3.236	3.409	3.634
total/unique,R_{int}	20007	20654/701, 0.040	21351	10532	8935	9720
GOF	1.040	1.003	1.082	1.048	1.097	1.075
R1[a]/wR2[b]	0.0359/0.1217	0.0398/0.1368	0.0270/0.0877	0.0705/0.1903	0.0788/0.2516	0.0656/0.1999

	2d	2e	3a	3b	3c	3d	3e
formula	$C_{24}H_{48}Eu_2Cd_3O_{42}$	$C_{24}H_{42}Dy_2Cd_3O_{39}$	$C_{24}H_{48}Dy_2Cd_3O_{42}$	$C_{24}H_{60}Ho_2Cd_3O_{48}$	$C_{24}H_{60}Er_2Cd_3O_{48}$	$C_{24}H_{60}Tm_2Cd_3O_{48}$	$C_{24}H_{60}Lu_2Cd_3O_{48}$
M_r	1649.77	1616.80	1670.85	1783.80	1783.80	1791.81	1803.87
T (K)	298(2)	298(2)	293(2)	293(2)	293(2)	293(2)	293(2)
cryst syst	hexagonal	hexagonal	cubic	cubic	cubic	cubic	cubic
space group	$P6/mcc$	$P6/mcc$	$Fd\bar{3}c$	$Fd\bar{3}c$	$Fd\bar{3}c$	$Fd\bar{3}c$	$Fd\bar{3}c$
a (Å)	12.7695(16)	12.6250(18)	26.2522(13)	26.179(3)	26.160(3)	26.124(3)	26.026(2)
b (Å)	12.7695(16)	12.6250(18)	26.2522(13)	26.179(3)	26.160(3)	26.124(3)	26.026(2)
c (Å)	17.727(3)	17.852(4)	26.2522(13)	26.179(3)	26.160(3)	26.124(3)	26.026(2)
α (deg)	90	90	90	90	90	90	90
β (deg)	90	90	90	90	90	90	90
γ (deg)	120	120	90	90	90	90	90
V (Å^3)	2503.3(6)	2464.2(7)	18092(3)	17942(6)	17903(6)	17829(6)	17629(4)
Z	2	2	16	16	16	16	16
D_{calcd} (mg/cm^3)	2.189	2.173	2.440	2.597	2.618	2.652	2.682
μ (mm^{-1})	3.836	4.379	4.776	5.029	5.255	5.493	6.008
total/unique,R_{int}	8997	11214	23002	24325	22706	33944	22112
GOF	1.179	1.043	1.014	1.018	1.087	1.038	1.043
R1[a]/wR2[b]	0.0713/0.2038	0.0848/0.2677	0.0682/0.2550	0.0519/0.1940	0.0547/0.2379	0.0506/0.2262	0.0640/0.2778

[a] $R1 = \sum||F_o| - |F_c||/\sum|F_o|$. [b] $wR2 = \{\sum w(|F_o|^2 - |F_c|^2)|/\sum|w(F_o)^2\}^{1/2}$.

and these should be handled with caution. The complexes described in this report have, so far, been found to be safe when used in small quantities.

2.1. Materials and Instrumentation. The organic solvents used in this manuscript were treated before the experiment according to the methods reported by Armarego and Chai.[7] $Ln(ClO_4)_3{\cdot}6H_2O$ was synthesized by dissolving lanthanide oxide in an excess amount of perchlorate acid. Other starting materials were of commercial origin and were used as received. The C, H, and N microanalyses were carried out with an Elementar Vario EL analyzer. The IR spectrum was recorded on a Nicolet FT-170SX instrument using KBr disks in the 400−4000 cm^{-1} region. Thermogravimetric analysis (TGA) was made on a P. E. Diamond TG/DTA/SPAECTRUN ONE thermal analyzer

dx.doi.org/10.1021/ic403080n | Inorg. Chem. 2014, 53, 5922−5930

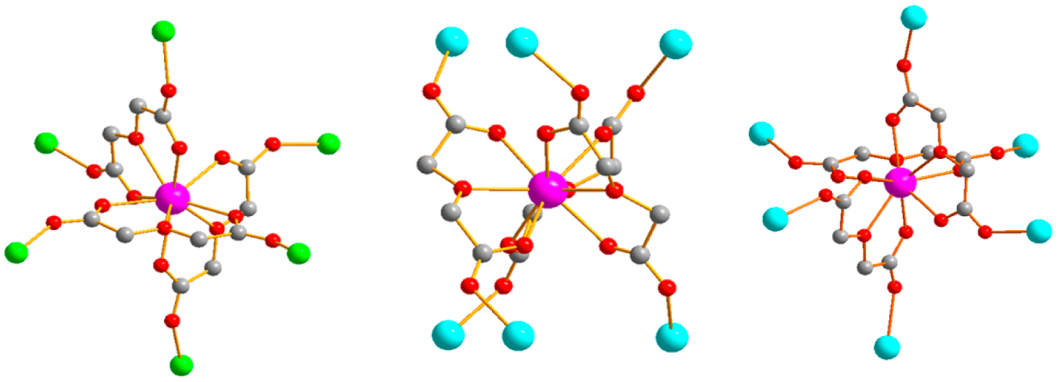

Figure 1. From left to right: anti−anti, syn−anti, and anti−anti conformations of a lanthanide metalloligand in **1**−**3**, respectively. Color code: magenta, Ln; green, Co; cyan, Cd; red, O; dark gray, C.

under a N_2 atmosphere with a heating rate of 5 °C/min. Powder X-ray diffraction (PXRD) and in situ PXRD patterns were obtained on Rigaku D/Max-II and D-Max 2000 VPC X-ray diffractometers with graphite-monochromatized Cu Kα radiation, respectively. The CO_2 adsorption isotherm was measured on an ASAP 2020 instrument. Fluorescence measurements were made on a Hitachi F-7000 spectrofluorimeter. Luminescent quantum yields and lifetimes were determined on a FLS920 instrument of Edinburgh Instrument. All of the measurements were done at room temperature. Magnetic susceptibility data were collected in the temperature range of 1.8−300 K in an applied field of 100 Oe by using a Quantum Design model MPMS-XL SQUID magnetometer. Pascal's constants were used to determine the diamagnetic corrections. Electron paramagnetic resonance (EPR) measurements were performed by using an X-band spectrometer (f = 9 GHz; JEOL JES-FA300).

Synthesis of $\{[Co(H_2O)_6]\cdot[Ln_2(ODA)_6Co_2]\cdot 6H_2O\}_n$ ***(1)***. A mixture of $Ln(OH)_3$ [Ln = Gd (**1a**), Dy (**1b**), and Er (**1c**); 0.5 mmol], H_2ODA (201 mg, 1.5 mmol), and $Co(ClO_4)_2\cdot 6H_2O$ (0.75 mmol) in H_2O (15 mL) was sealed in a 25 mL Teflon-lined bomb at 170 °C for 7 days and then slowly cooled to room temperature at a cooling rate of 5 °C/h. Deep-red cubic crystals of complex **1** were obtained (yields of **1a**−**1c**: 75%, 78%, and 77%, respectively, based on Ln). Elem anal. Found (calcd) for $C_{24}H_{48}Gd_2Co_3O_{42}$ (**1a**): C, 19.15 (19.22); H, 3.35 (3.23). Found (calcd) for $C_{24}H_{48}Dy_2Co_3O_{42}$ (**1b**): C, 19.03 (19.08); H, 3.27 (3.20). Found (calcd) for $C_{24}H_{48}Er_2Co_3O_{42}$ (**1c**): C, 19.02 (18.97); H, 3.23 (3.18). IR (KBr, cm^{-1}): (**1a**) 3502(s), 1603(s), 1435(m), 1358(m), 1310(m), 1122(m), 1049(m), 938(m), 736(w), 563(w); (**1b**) 3500(s), 1605(s), 1436(m), 1359(m), 1311(m), 1127(m), 1051(m), 940(m), 736(w), 565(w); (**1c**) 3503(s), 1607(s), 1437(m), 1359(m), 1310(m), 1131(m), 1053(m), 942(m), 738(w), 567(w).

Synthesis of $\{[Ln_2(ODA)_6Cd_3(H_2O)_6]\cdot mH_2O\}_n$ ***(2)***. A mixture of $Ln(ClO_4)_3\cdot 6H_2O$ [Ln = Pr (**2a**), Nd (**2b**), Sm (**2c**), Eu (**2d**), and Dy (**2e**); 0.5 mmol] and H_2ODA (201 mg, 1.5 mmol) was added to 10 mL of H_2O under vigorous stirring. The pH value of the reaction mixture was adjusted to about 6.0 by the slow addition of a 0.1 M NaOH solution, and the solution was stirred for 1 h at room temperature. Then $Cd(ClO_4)_2\cdot 2H_2O$ (314 mg, 0.75 mmol) was added, and the pH value of the reaction mixture was again adjusted to 6.5 by the addition of a 0.1 M NaOH solution. After 4 h of stirring at 60 °C, the solution was filtered and left at room temperature. Colorless prismatic crystals were obtained after 2 weeks (yields of **2**: all above 95%, based on Ln). Elem anal. Found (calcd) for $C_{24}H_{54}Pr_2Cd_3O_{45}$ (**2a**, m = 9): C, 17.20 (17.14); H, 3.29 (3.24). Found (calcd) for $C_{24}H_{48}Nd_2Cd_3O_{42}$ (**2b**, m = 6): C, 17.70 (17.64); H, 3.04 (2.96). Found (calcd) for $C_{24}H_{48}Sm_2Cd_3O_{42}$ (**2c**, m = 6): C, 17.47 (17.51); H, 2.99 (2.94). Found (calcd) for $C_{24}H_{48}Eu_2Cd_3O_{42}$ (**2d**, m = 6): C, 17.50 (17.47); H, 2.98 (2.93). Found (calcd) for $C_{24}H_{42}Dy_2Cd_3O_{39}$ (**2e**, m = 3): C, 17.77 (17.83); H, 2.69 (2.62). IR (KBr, cm^{-1}): (**2a**) 423(s), 1597(s), 1427(m), 1358(m), 1315(m), 1118(m), 1044(m), 932(m), 707(w), 604(w), 565(w); (**2b**) 3568(s), 1608(s), 1432(m), 1358(m), 1312(m), 1118(m), 1042(m), 934(m), 721(w), 608(w), 571(w); (**2c**) 3571(s), 1607(s), 1438(m), 1359(m), 1313(m), 1120(m), 1042(m), 936(m), 721(w), 610(w), 571(w); (**2d**) 3573(s), 1608(s), 1438(m), 1359(m), 1313(m), 1122(m), 1042(m), 937(m), 721(w), 610(w), 572(w); (**2e**) 3469(s), 1596(s), 1435(m), 1360(m), 1315(m), 1126(m), 1046(m), 933(m), 732(w), 603(w), 563(w).

Synthesis of $\{[Cd(H_2O)_6]\cdot[Ln_2(ODA)_6Cd_2]\cdot mH_2O\}_n$ ***(3)***. The complexes were prepared by the same method as that of **1**, using $Cd(ClO_4)_2\cdot 2H_2O$ instead of $Co(ClO_4)_2\cdot 6H_2O$. Colorless cubic crystals of complex **3** were obtained (yields of **3**: all above 90%, based on Ln). Elem anal. Found (calcd) for $C_{24}H_{48}Dy_2Cd_3O_{42}$ (**3a**, m = 6): C, 17.28 (17.25); H, 2.93 (2.90). Found (calcd) for $C_{24}H_{60}Ho_2Cd_3O_{48}$ (**3b**, m = 12): C, 16.20 (16.16); H, 2.43 (3.39). Found (calcd) for $C_{24}H_{60}Er_2Cd_3O_{48}$ (**3c**, m = 12): C, 16.16 (16.12); H, 3.43 (3.38). Found (calcd) for $C_{24}H_{60}Tm_2Cd_3O_{48}$ (**3d**, m = 12): C, 16.13 (16.09); H, 3.32 (3.38). Found (calcd) for $C_{24}H_{60}Lu_2Cd_3O_{48}$ (**3e**, m = 12): C, 16.04 (15.98); H, 3.43 (3.35). IR (KBr, cm^{-1}): (**3a**) 3500(s), 1605(s), 1436(m), 1359(m), 1310(m), 1126(m), 1051(m), 940(m), 736(w), 565(w); (**3b**) 3502(s), 1605(s), 1437(m), 1359(m), 1311(m), 1129(m), 1052(m), 941(m), 737(w), 566(w); (**3c**) 3503(s), 1607(s), 1437(m), 1358(m), 1310(m), 1129(m), 1052(m), 942(m), 738(w), 567(w); (**3d**) 3500(s), 1605(s), 1438(m), 1359(m), 1310(m), 1133(m), 1054(m), 943(m), 739(w), 567(w); (**3e**) 3499(s), 1607(s), 1438(m), 1359(m), 1310(m), 1135(m), 1054(m), 949(m), 739(w), 568(w).

2.2. Single-Crystal X-ray Diffraction Analysis. The collection of crystallographic data was carried out on a Bruker SMART-1000 CCD area detector diffractometer with graphite-monochromated Mo Kα radiation (λ = 0.71073 Å). All structures were solved by direct methods and refined by full-matrix least-squares methods on F^2 using the *SHELXTL* crystallographic software package.[8] Anisotropic thermal parameters were used to refine all non-hydrogen atoms. Hydrogen atoms were located geometrically and refined isotropically. The crystal data and structure refinement details are summarized in Table 1. Selected bond lengths and angles for all compounds are given in Table S1 in the Supporting Information (SI).

3. RESULTS AND DISCUSSION

3.1. Synthesis of the Title Complexes. Control experiments showed that by using $Ln(ClO_4)_3$ as a raw material one could not get the single crystals of **1** and **3** and by using Ln_2O_3 one could get **1** and **3** but yields were extremely low (<5%, based on Ln). However, by using $Ln(OH)_3$ one could obtain **1** and **3** with high yield (>75% for **1** and >90% for **3**). Meanwhile, using a "one-pot" method to synthesize **2** ended in very low yield (<15%). The above results indicated that the formation of a lanthanide metalloligand was the first step to assembling the title complexes.

3.2. Crystal Structures of 1−3. X-ray determination reveals that complexes **1** and **3** crystallize in the cubic crystal

dx.doi.org/10.1021/ic403080n | *Inorg. Chem.* 2014, 53, 5922−5930

system with space group $Fd\bar{3}c$ and crystals of complex **2** are in the hexagonal space group *P6/mcc*. In all compounds, the metalloligand $[Ln(ODA)_3]^{3-}$ acts as a hexadentate ligand to bond six TM^{II} ions (Co^{2+} in **1** or Cd^{2+} in **2** and **3**) in different conformations, which are syn−anti in complex **2** and anti−anti in complexes **1** and **3** (Figure 1).

Complexes **1** and **3** are isostructural. For the sake of brevity, therefore, the crystal structures of compounds **1a** and **3b** are depicted here in detail. In **1a** and **3b**, the Co^{II} (**1a**) and Cd^{II} (**3b**) of the frameworks are surrounded by six oxygen atoms from six metalloligands to form light distorted octahedral configurations. The bond lengths of Co−O and Cd−O are 2.095 and 2.267 Å, respectively. The bond angles of O−Co−O are 87.07°, 92.93°, and 180.00° in **1a**. The corresponding contents in **3b** are 87.37°, 92.63°, and 180.00°. The coordination geometry of a lanthanide metalloligand can be described as a distorted bicapped tetrahedron in complexes **1a** and **3b**. It is worth noting that a perfect octahedron was formed by a lanthanide metalloligand and six TM^{II} ions (Figure 2)

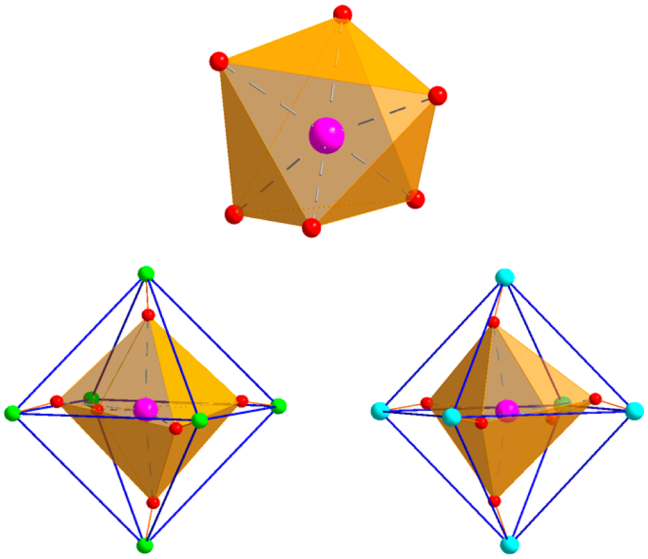

Figure 2. From top to bottom: coordination geometry of a lanthanide metalloligand and the perfect octahedron formed by a metalloligand with TM in **1** and **3**. Color code: magenta, Ln; green, Co; cyan, Cd; red, O.

through the TM−O bonds, in which the Ln^{III} ion occupied the geometric body center of the octahedron and the angle of TM−O···Ln is 154.50° (Co−O···Gd) or 153.34° (Cd−O···Ho). In the octahedron, the angles of TM···Ln···TM and TM···TM···TM are 90.00°/ 180.00° and 60.00°/90.00°, respectively. The distances of Ln···TM and the adjacent TM···TM are 6.440 Å (Gd···Co) and 9.108 Å (Co···Co) in **1a** and 6.545 Å (Ho···Cd) and 9.256 Å (Cd···Cd) in **3b**. *PLATON*[9] calculations indicated void volumes of 23.3% and 23.7% for **1a** and **3b**, respectively (guest water molecules and counterions are not included in the calculations).

Single-crystal X-ray diffraction studies of complex **2** revealed that these complexes are isomorphic. Herein, we use complex **2d** as a representative example to discuss the structure in detail. Each Cd^{2+} ion is coordinated by two oxygen atoms from two water molecules in the axial positions (Cd−O, 2.273 Å) and four oxygen atoms from four metalloligands in the equatorial positions (Cd−O, 2.249 Å), giving a distorted octahedron with two axial bonds elongated lightly. The bond angles of O−Cd−O range from 83.66° to 180.00°. As shown in Figure 3, the

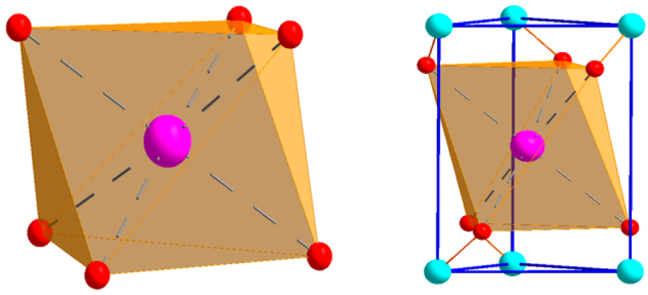

Figure 3. Coordination geometry of a lanthanide metalloligand (left) and the regular triprism formed by a metalloligand with Cd^{II} in **2**. Color code: magenta, Ln; cyan, Cd; red, O.

lanthanide metalloligand adopts a lightly distorted trigonal-antiprismatic geometry bonded with six Cd^{2+} ions by Cd−O bonds, in which the angle of Cd−O···Eu is about 113.42°, to give rise to a regular triprism, and the Eu^{III} ion is located at the geometric body center. In the triprism, the distances of the adjacent Cd···Cd are 6.385 and 8.864 Å and the angles of Cd···Cd···Cd are 60.00° and 90.00°, respectively. The distance of Eu···Cd is 5.764 Å, and the angles of Cd···Eu···Cd range from 67.26° to 142.72°. More importantly, as a result of falling into a D_{6h} point group, the Eu^{III} ions in **2d** have a highly symmetric coordination environment with an inversion center. The potential free volume of the complex is about 527.5 $Å^3$, comprising 21.1% of the crystal volume, as calculated by *PLATON*[9] (guest water molecules are not included in the calculations).

Topological analysis shows that complexes **1** and **3** presented a typical NaCl topology with 3-fold interpenetration 3D anionic channels about 6 × 6 Å, in which $[Co(H_2O)_6]^{2+}$ and $[Cd(H_2O)_6]^{2+}$ act as counterions filling in it, and complex **2** had a honeycomblike $(6^4,4^4)$-connected net with ∼1.2-nm-diameter 1D neutral hydrophilic channels (Figures 4 and S1 in the SI). The pore diameter and volume of **2** are listed in Table S2 in the SI.

Furthermore, complexes **2e**, $\{[Dy_2(ODA)_6Cd_3(H_2O)_6]\cdot 3H_2O\}_n$, and **3a**, $\{[Cd(H_2O)_6]\cdot[Dy_2(ODA)_6Cd_2]\cdot 6H_2O\}_n$, could be termed framework isomers owing to the different conformations of the lanthanide metalloligand, which is a rare example of a 3D d−f HMOF.[4c,10]

3.3. TGA and PXRD of 1−3. The existence of guest water molecules in the microporous frameworks inspired us to investigate the thermal stability of complex **2**. The experiments for crystal samples **2b−2e** were performed from 23 to 670 °C. The TGA curves for **2b−2e** (Figure 5a) show a weight loss of about 11.40% from 23 to 165 °C, corresponding to the loss of both the guest and coordinated water molecules (calcd 11.66%). There is no obvious weight loss from 165 to 305 °C, and after that, complex **2** begins to chemically decompose. Guest water molecules were removed by heating **2d** at 200 °C under a vacuum for 24 h, and then the guest-free sample of $[Eu_2Cd_3(ODA)_6]_n$ (**2D**) was prepared. To further test the stability of the host framework after the guest water molecules were removed, we examined the sample of as-synthesized **2d** by in situ PXRD analysis from 25 to 300 °C. The result of in situ PXRD shows that the host framework was stable throughout the test temperature interval (Figure 5b). It is worth noting that

dx.doi.org/10.1021/ic403080n | *Inorg. Chem.* 2014, 53, 5922−5930

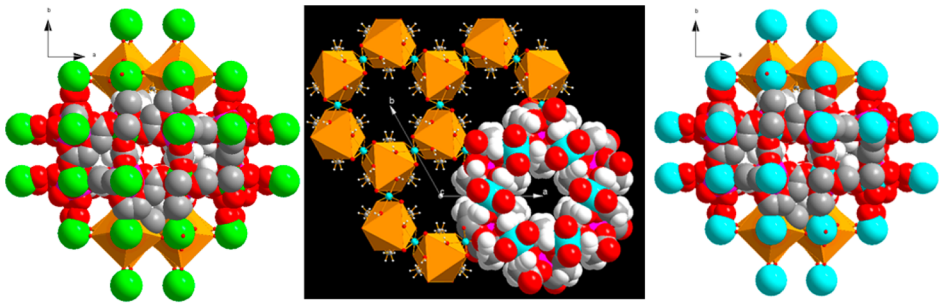

Figure 4. Packing view of **1** (left), **2** (middle), and **3** (right) along the *c* axis. Color code: magenta, Ln; green, Co; cyan, Cd; red, O; white, H; gray, C. Orange polyhedron: lanthanide metalloligand. Guest water molecules and counterions were omitted for clarity.

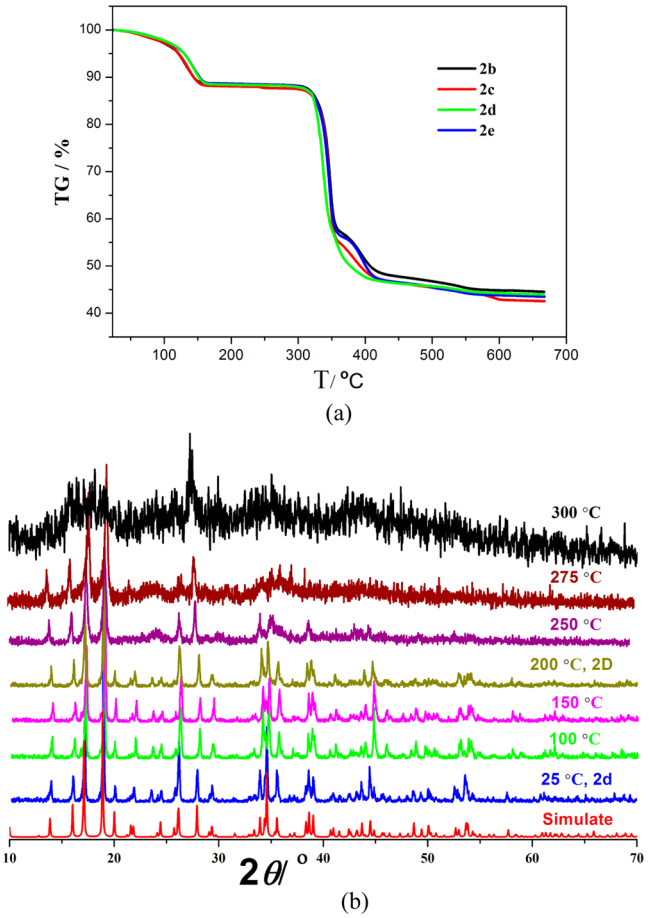

Figure 5. (a) TGA curves of **2b**–**2e**. (b) In situ PXRD pattern of **2d** from 25 to 300 °C: **2d**, as-synthesized, blue; **2D**, dark yellow.

the patterns of **2d** and **2D** are nearly identical; only the intensities of some peaks varied, which supports the notion that the framework remains intact after the guest water molecules are removed. At the same time, the permanent porosity of **2D** was established by CO_2 sorption at 273 K, which showed obvious CO_2 adsorption into the pores (22 $cm^3\ g^{-1}$ at 1.2 atm; Figure S2 in the SI).

Because of the structural similarity, the as-synthesized compounds **1** and **3** (**3a**–**3e**) experienced similar thermal processes in TGA (Figure 6). Continuing weight losses below 285 °C for **1** and 240 °C for **3** correspond to the loss of all lattice and coordinated water molecules. The average weight losses are about 10.42% (**1**) and 9.49% (**3**), in agreement with the calculated values of 10.58% (**1**) and 9.72% (**3**) for the total water molecules per formula. Also, no further weight loss happens from 285 to 325 °C for **1** and from 245 to 345 °C for **3**. Upon further heating, the striking weight loss above 350 °C for **1** and **3** is attributed to decomposition of the dehydrated phases. To confirm the phase purity of complexes **1** and **3**, the PXRD patterns were carried out at room temperature (Figure S3a in the SI). The diffraction peaks of the as-synthesized samples are well in agreement with the simulated data, demonstrating the high phase purity of the compounds. Furthermore, as representatives, in situ PXRD of **1c** and **3c** shows that the complexes still maintain the initial structure over at least 300 and 325 °C, respectively (Figure S3b in the SI).

By comparison of the TGA curves of complexes **1b**, **2e**, and **3a** (Figure 7), two thermostability rules of the title complexes were found. First, the higher the symmetry of the complex, the higher the degradation temperature will be. As mentioned above, complex **2e** belongs to the D_{6h} point group, while complexes **1b** and **3a** fall into the O_h point group. It is obvious that the symmetry of **2e** is lower than that of **1b** and **3a**; in contrast, the degradation temperature of **2e** is 305 °C, which is

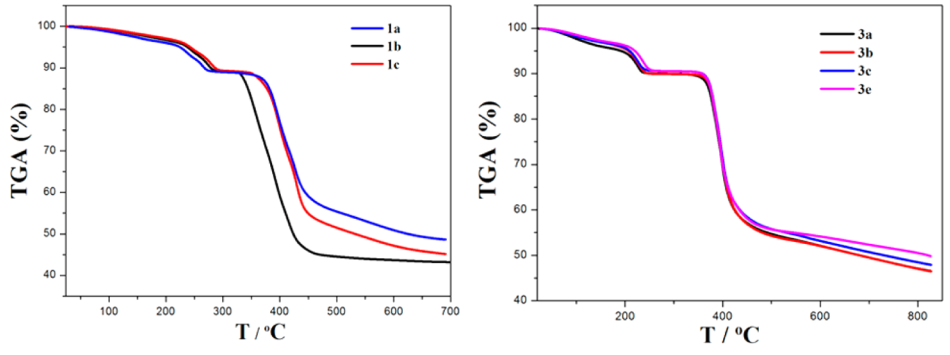

Figure 6. TGA curves of **1** (left) and **3** (right).

dx.doi.org/10.1021/ic403080n | *Inorg. Chem.* 2014, 53, 5922–5930

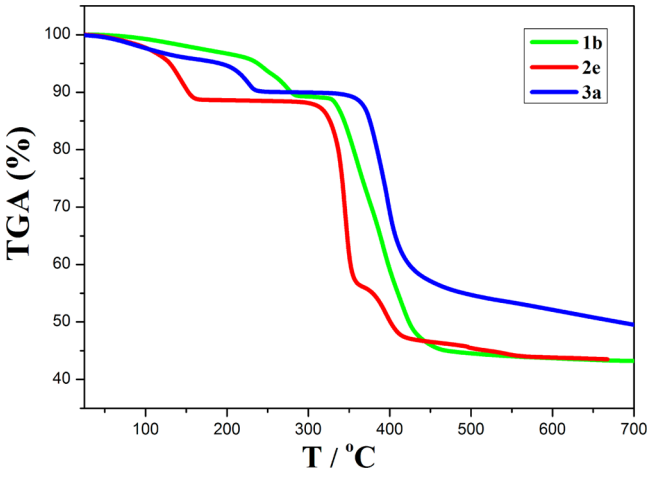

Figure 7. TGA curves of **1b**, **2e**, and **3a**.

lower than 325 °C (**1b**) and 345 °C (**3a**). Second, the larger the ionic radius of TM^{II}, the larger the thermostable interval will be. Because the ionic radius of Cd^{II} is larger than that of Co^{II}, the capacity of the TM−O bond extension to antagonize thermal expansion in **2e** and **3a** is stronger than that of **1b**. Therefore, the thermostable intervals for **2e** (165−305 °C) and **3a** (245−345 °C) are wider than that of **1b** (285−325 °C).

3.4. Guest Molecule Exchange of 2d. Complex **2d** has poor solubility in most organic solvents, and as revealed by the crystal structure, the guest water molecules were filled in the pores and there was no strong interaction with the host frameworks, which indicates that the guest water molecules might be replaced by other molecules under appropriate conditions. Additionally, the channels in **2d** are neutral and hydrophilic, so the water-miscible small organic molecules, such as methanol (MeOH), ethanol (EtOH), propanol (PrOH), acetone, acetonitrile, *N*,*N*-dimethylformamide, tetrahydrofuran, 1,4-dioxane, and so on, were chosen as guest molecules (**G**) to investigate the guest exchange of **2d**. The guest-free phase **2D** (100 mg) was placed in 20 mL of the guest solvent and refluxed for 4 h with vigorous stirring and then cooled to room temperature. After 3 days of immersion, **2D+G** was obtained by filtering and air-dried. Elemental analysis and TGA revealed that a unit formula of the host could be filled with about 2.5 molecules of EtOH, 4.3 molecules of MeOH, 1.6 molecules of acetone, and 2 molecules of PrOH as well as a pyridine molecule (Figure S4 and Table S3 in the SI). Regenerated **2D** was obtained from heating **2D+G** at 180 °C under a vacuum for 24 h. **2d** was obtained again by placing **2D** in water for 2 days or exposing **2D** to air for several days. PXRD (Figure S5 in the SI) of the transformation between **2d**, **2D**, and **2D+G** showed that the hydrophilic small organic molecules could access the pores freely without structural changes, which verified that guest molecules have no strong interaction with the host network.

3.5. Magnetic Properties of 1. The magnetic behavior of **1a**−**1c** was studied on polycrystalline samples (Figures 8−10). As shown in Figure 8, the observed $\chi_M T$ value for **1a** at 300 K is 23.81 cm^3 K mol^{-1}, which is slightly higher than 21.39 cm^3 K mol^{-1} expected for two isolated Gd^{III} ions ($^8S_{7/2}$, g = 2.0) and three spin-only isolated Co^{II} ions ($S = {}^3/_2$, g = 2.0). This is attributed to the significant orbital contributions of the distorted octahedral high-spin Co^{2+} ions.[11]

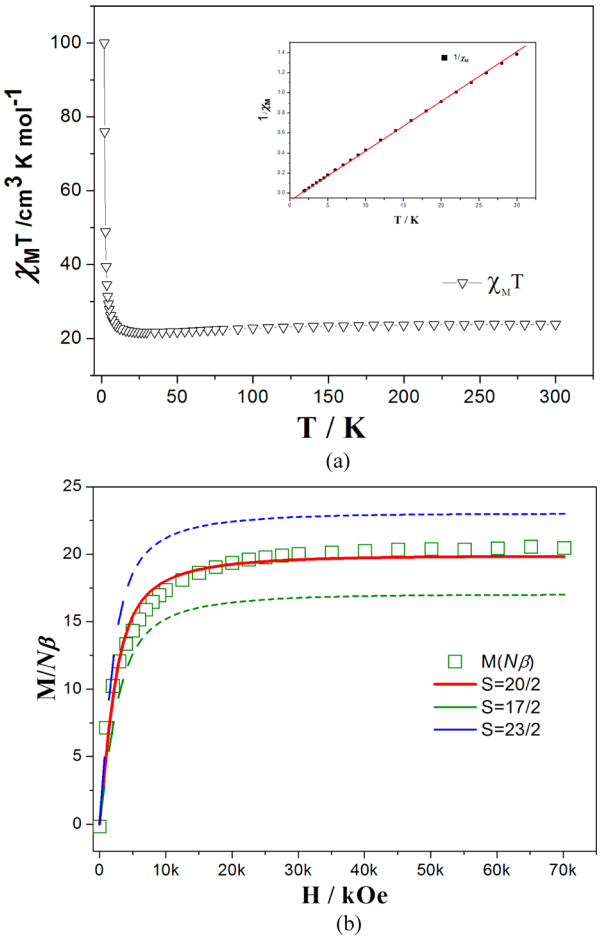

Figure 8. (a) Thermal dependence of the $\chi_M T$ curves of **1a** (the inset is the Curie−Weiss fitting). (b) M versus H data at 1.8 K with the theoretical Brillouin curve.

$\chi_M T$ decreased slowly from 300 K and reached a minimum of 21.68 cm^3 K mol^{-1} at ca. 30 K. Upon further cooling, a sharp increase was observed. The $\chi_M T$ value at 1.8 K was 99.94 cm^3 K mol^{-1}, indicating the presence of ferromagnetic interactions between the metal centers via the bridging ligands in the 3D structure, which is further supported by the well-fitted $\chi_M{}^{-1}$ versus T plot that gives C = 20.53 cm^3 mol^{-1} K and θ = 1.33 K (Figure 8a, inset). The field dependence of the magnetization (0−70 kOe) measured at 1.8 K (Figure 8b) shows an initial rapid increase for fields up to 20 kOe, reaching 19.34 Nβ and then 20.44 Nβ at 70 kOe. The theoretical Brillouin curves (eqs 1−3) for $S = {}^{17}/_2$, $S = {}^{20}/_2$, and $S = {}^{23}/_2$ spin ground states ($S_{Gd} = {}^7/_2$, g_{Gd} = 2.0; $S_{Co} = {}^3/_2$, g_{Co} = 2.0) were used to fit the experimental curve.

$$M = NgS\mu_B B_s(x) \ldots \quad (1)$$

$$B_s(x) = \frac{2S+1}{2S}\coth\left(\frac{2S+1}{2S}x\right) - \frac{1}{2S}\coth\left(\frac{1}{2S}x\right) \ldots \quad (2)$$

$$x = \frac{g\mu_B}{kT}H \ldots \quad (3)$$

The results show that the $S = {}^{20}/_2$ spin state (two noninteracting S_{Gd} and two noninteracting S_{Co}) fits well. This means that the counterions, $[Co(H_2O)_6]^{2+}$, have not contributed to the host framework and just act as paramagnetic

dx.doi.org/10.1021/ic403080n | Inorg. Chem. 2014, 53, 5922−5930

ions to be filled in the 3D anionic channels. What is more, the experimental curve lies above the $S = {}^{20}/_{2}$ spin state, which also supports the presence of intermetallic Gd---Gd/Co ferromagnetic coupling in **1a** resulting from the anti−anti conformation of the acetate bridge.[12] As expected, owing to the isotropic character of the Gd^{III} ion ($4f^{7}$), the different directions of the applied field and the field sweep rate studies at 2 K did not show any significant hysteresis effect (Figure S6a in the SI).[13] The zero-field alternating-current susceptibility was also measured with different frequencies (10−997 Hz) at 2−10 K. However, no frequency dependence and magnetic ordering were observed (Figure S6b in the SI).

Complexes **1b**[14] and **1c** have room temperature $\chi_M T$ values of 42.31 and 36.38 cm^3 K mol^{-1}, close to the values calculated for noninteracting ions, 38.71 cm^3 K mol^{-1} [for two Dy^{3+}, $g_J = {}^{4}/_{3}$, and ${}^{6}H_{15/2}$, and for three Co^{2+}, $g = 2.79$ (Figure 9 inset)

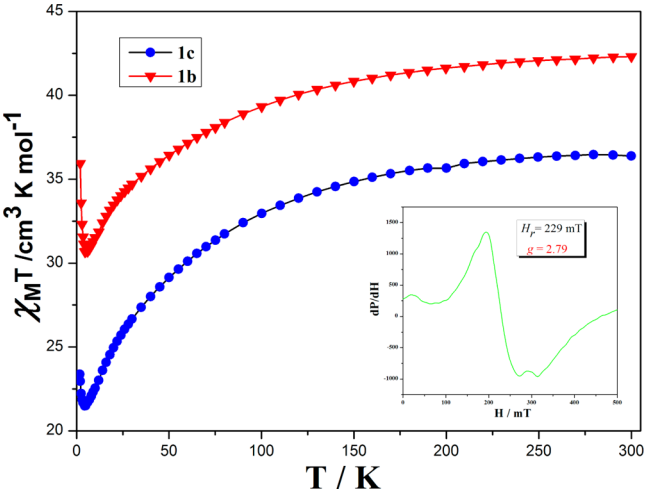

Figure 9. Curves of $\chi_M T$ versus T for **1b** and **1c**. Inset: EPR spectrum of **1b** at room temperature, which shows the g value of Co^{2+} ions in **1b**.

and $S = {}^{3}/_{2}$] and 33.22 cm^3 K mol^{-1} (for two Er^{3+}, $g_J = {}^{6}/_{5}$ and ${}^{4}I_{15/2}$, and for three Co^{2+}, $g = 2.7$ and $S = {}^{3}/_{2}$).[15] Upon lowering of the temperature, the $\chi_M T$ values for the two complexes slowly decrease to 125 K and sharply drop to reach minima at 6 K for **1b** and at 8 K for **1c**, which were ascribed to thermal depopulation of the excited Stark levels of Ln^{III} ions [Ln = Dy (**1b**) and Er (**1c**)] and the spin−orbit coupling of the single-ion behavior of Co^{II} ions[15c] (Figure 9). With the temperature continuously decreasing to 1.8 K, the $\chi_M T$ values of the two complexes have an upturn and reach maxima of 35.94 cm^3 K mol^{-1} for **1b** and 23.38 cm^3 K mol^{-1} for **1c**, indicating Ln---Ln/Co ferromagnetic interactions. The interactions are strong enough to compensate for thermal depopulation of the excited Stark levels and the single-ion behavior resulting from spin−orbit coupling.[16] The magnetic susceptibility data of **1b** and **1c** below 6 and 8 K (Figure S7 in the SI) obey the Curie−Weiss law with $C = 27.56$ cm^3 mol^{-1} K, $\theta = 0.45$ K and $C = 20.41$ cm^3 mol^{-1} K, $\theta = 0.22$ K, respectively. The positive θ values support ferromagnetic interactions between the metal ions. The molar magnetizations (M) as a function the applied magnetic field (H) of the two complexes at 1.8 K rise to values of 17.67Nβ (**1b**) and 18.04 Nβ (**1c**) at 70 kOe without achieving saturation (Figure 10).

The lack of saturation on the M versus H data at 1.8 K may be explained as the presence of a significant magnetic anisotropy and/or the lack of a well-defined ground state, suggesting the presence of low-lying excited states that might be populated when a field is applied.[17]

Because the Co^{II} and Ln^{III} ions both possess intrinsic complicated magnetic characteristics including spin−orbit coupling and magnetic anisotropy,[18] we give up any attempt to quantificationally analyze the coupling interactions between Ln---Ln/Co in the 3D HMOFs of **1**.

3.6. Guest-Induced Luminescent Properties of 2d.

Because of the excellent luminescent properties of Eu^{III} ions, solid-state photoluminescence of complex **2d** was investigated at room temperature. The emission spectrum of **2d** (excited at 397 nm) exhibits the three main characteristic emissions of the Eu^{3+} ions. Three intense peaks at 592, 618, and 696 nm correspond to a transition between the first excited state ${}^{5}D_0$ and the ground multiplet ${}^{7}F_J$ (J = 1, 2, and 4) for Eu^{3+} ions (Figure 11). The fluorescence quantum yield and lifetime of the ${}^{5}D_0$ level in **2d** were found to be 22.91 ± 0.3% and 1.94 ms, respectively. The most remarkable feature of **2d** is that the intensity of the ${}^{5}D_0 \rightarrow {}^{7}F_1$ transition is 3 times more than that of the ${}^{5}D_0 \rightarrow {}^{7}F_2$ transition. It is well-known that the ${}^{5}D_0 \rightarrow {}^{7}F_1$ transition is a magnetic-dipole transition and its intensity varies with the crystal-field strength acting on the Eu^{3+} ions. On the other hand, the ${}^{5}D_0 \rightarrow {}^{7}F_2$ transition is an electric-dipole transition, and its transition intensity decreases as the site symmetry of Eu^{III} increases. Furthermore, the symmetry-forbidden emission ${}^{5}D_0 \rightarrow {}^{7}F_0$ transition was not observed at 580 nm, revealing that the Eu^{III} ions in **2d** occupy sites with high symmetry.[18b,19] The result of solid-state photoluminescence of **2d**, thus, indicates the presence of an inversion center at the Eu^{III} site, which is in agreement with the result of single-crystal X-ray analysis. This was rarely observed before for

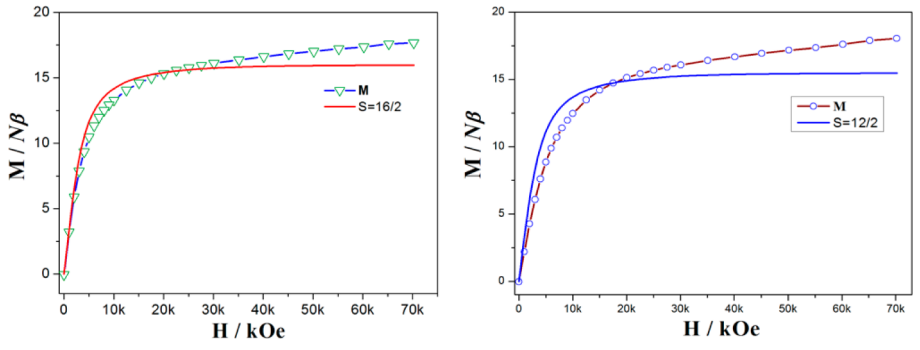

Figure 10. M versus H data at 1.8 K with the theoretical Brillouin curves of **1b** (left) and **1c** (right).

dx.doi.org/10.1021/ic403080n | Inorg. Chem. 2014, 53, 5922−5930

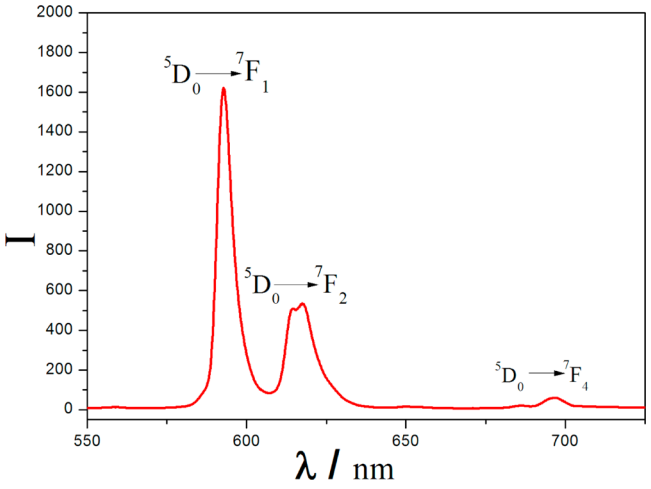

Figure 11. Luminescent spectrum of **2d** excited at 397 nm.

lanthanide and d−f heterometallic frameworks to our best knowledge.

As described above, **2d** could "breathe" hydrophilic small organic molecules. To examine the guest-dependent luminescent properties of **2d**, the luminescence properties of **2D+G** were investigated. As shown in Figure 12, the photo-

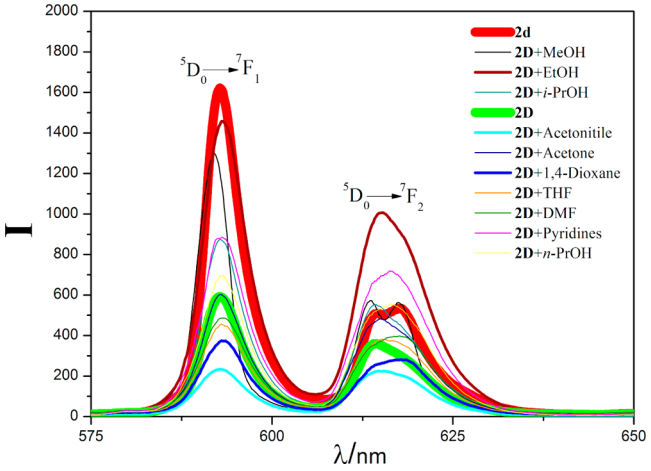

Figure 12. Guest-induced luminescent properties of **2D+G** excited at 397 nm.

luminescence spectrum (excited at 397 nm) has obviously changed when the guest molecules entered into the channels. First, the emission intensity of **2d** is significantly stronger than **2D**, implying that water molecules sensitize the luminescence.[20] Second, all of the guest molecules reduce the emission intensity of the $^5D_0 \rightarrow {}^7F_1$ transition, which is hypersensitive to the ligand environment. Except for acetonitrile and 1,4-dioxane, almost all guest molecules enhance the emission intensity of the $^5D_0 \rightarrow {}^7F_2$ transition, especially EtOH. These results suggest that the geometry of the first coordination sphere of the Eu^{III} ions is slightly distorted,[20,21] while the guest molecules are inside the channels. However, the present intensity ratio $I(^5D_0 \rightarrow {}^7F_1)/I(^5D_0 \rightarrow {}^7F_2)$ is always >1 (Figure 13), which could result from the Eu^{III} ions still being placed in a fundamentally symmetric environment.

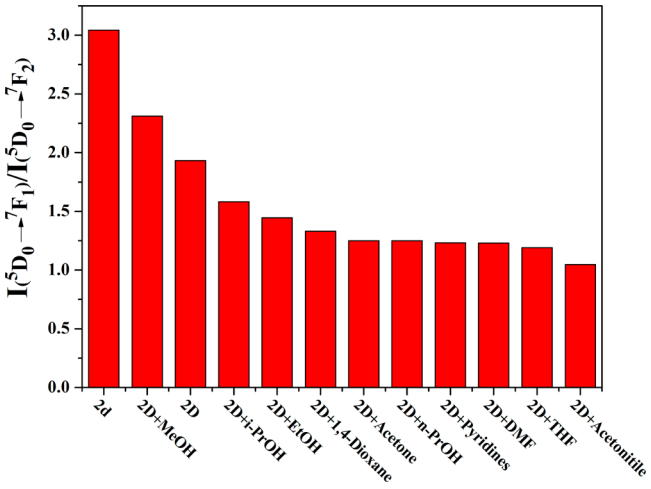

Figure 13. Intensity ratios $I(^5D_0 \rightarrow {}^7F_1)/I(^5D_0 \rightarrow {}^7F_2)$ of **2d**, **2D**, and **2D+G**.

4. CONCLUSION

In summary, three series (**1**−**3**) of 3D d−f HMOFs based on lanthanide metalloligands were obtained by different synthesis methods. **1** and **3** are isostructural and represent a kind of anionic porous HMOF, which contains typical NaCl topology with 3-fold interpenetration. Magnetic studies of **1** show ferromagnetic interactions between the metal ions. In **2**, the Ln^{III} ions occupy an inversion center and water molecules that were filled into the 1D neutral channels can be exchanged by other hydrophilic small organic molecules. Notably, the characteristic emission of the Eu^{3+} ions in **2d** could change significantly upon the introduction of different guest molecules. The results presented herein not only prove that the lanthanide metalloligand strategy is an effective method to design and construct HMOFs but also expand the field of finding the new magnetic and luminescent materials for chemists.

■ ASSOCIATED CONTENT

Ⓢ Supporting Information

Crystallographic data (CIF) and additional supporting data. This material is available free of charge via the Internet at http://pubs.acs.org.

■ AUTHOR INFORMATION

Corresponding Author

*E-mail: liuws@lzu.edu.cn. Tel.: +86-931-8915151. Fax: +86-931-8912582.

Notes

The authors declare no competing financial interest.

■ ACKNOWLEDGMENTS

The authors acknowledge financial support from the NSFC (Grants 20931003, 91122007, and 21261018), the Specialized Research Fund for the Doctoral Program of Higher Education (Grant 20110211130002), and the NSF of Ningxia (Grant NZ13042), and the 2011 Research Fund of the University of Ningxia (Grant 411-0270).

■ REFERENCES

(1) (a) Sakamoto, M.; Manseki, K.; Okawa, H. *Coord. Chem. Rev.* **2001**, *219*−*221*, 379−414. (b) Plecnik, C. E.; Liu, S.; Shore, S. G. *Acc. Chem. Res.* **2003**, *36*, 499−508. (c) Shibasaki, M.; Yoshikawa, N. *Chem.*

Rev. **2002**, *102*, 2187−2210. (d) Das, M. C.; Xiang, S.; Zhang, Z.; Chen, B. *Angew. Chem., Int. Ed.* **2011**, *50*, 10510−10520.
(2) (a) Zhao, B.; Cheng, P.; Chen, X.; Cheng, C.; Shi, W.; Liao, D.; Yan, S.; Jiang, Z. *J. Am. Chem. Soc.* **2004**, *126*, 3012−3013. (b) Ren, Y.-P.; Long, L.-S.; Mao, B.-W.; Yuan, Y.-Z.; Huang, R.-B.; Zheng, L.-S. *Angew. Chem., Int. Ed.* **2003**, *42*, 532−535. (c) Huang, Y.-G.; Wang, X.-T.; Jiang, F.-L.; Gao, S.; Wu, M.-Y.; Gao, Q.; Wei, W.; Hong, M.-C. *Chem.—Eur. J.* **2008**, *14*, 10340−10347. (d) Pointillart, F.; Bernot, K.; Sessoli, R.; Gatteschi, D. *Chem.—Eur. J.* **2007**, *13*, 1602−1609. (e) Zhuang, G.-L.; Chen, W.-X.; Zhao, H.-X.; Kong, X.-J.; Long, L.-S.; Huang, R.-B.; Zheng, L.-S. *Inorg. Chem.* **2011**, *50*, 3843−3845. (f) Kou, H. Z.; Zhou, B. C.; Wang, R. J. *Inorg. Chem.* **2003**, *42*, 7658−7665. (g) Ma, J.-x.; Huang, X.-f.; Song, Y.; Song, X.-q.; Liu, W.-s. *Inorg. Chem.* **2009**, *48*, 6326−6328.
(3) Kumar, G.; Gupta, R. *Chem. Soc. Rev.* **2013**, *42*, 9403−9453.
(4) (a) Chandler, B. D.; Cramb, D. T.; Shimizu, G. K. H. *J. Am. Chem. Soc.* **2006**, *128*, 10403−10412. (b) Chandler, B. D.; Yu, J. O.; Cramb, D. T.; Shimizu, G. K. H. *Chem. Mater.* **2007**, *19*, 4467−4473. (c) Ma, J.-x.; Huang, X.-f.; Song, X.-q.; Liu, W.-s. *Chem.—Eur. J.* **2013**, *19*, 3590−3595.
(5) Cui, Y.; Yue, Y.; Qian, G.; Chen, B. *Chem. Rev.* **2012**, *112*, 1126−1162.
(6) (a) Rinck, J.; Novitchi, G.; Van den Heuvel, W.; Ungur, L.; Lan, Y.; Wernsdorfer, W.; Anson, C. E.; Chibotaru, L. F.; Powell, A. K. *Angew. Chem., Int. Ed.* **2010**, *49*, 7583−7587. (b) Peng, J.-B.; Zhang, Q.-C.; Kong, X.-J.; Zheng, Y.-Z.; Ren, Y.-P.; Long, L.-S.; Huang, R.-B.; Zheng, L.-S.; Zheng, Z. *J. Am. Chem. Soc.* **2012**, *134*, 3314−3317. (c) He, F.; Tong, M.-L.; Chen, X.-M. *Inorg. Chem.* **2005**, *44*, 8285−8292. (d) Cai, S.-L.; Zheng, S.-R.; Wen, Z.-Z.; Fan, J.; Wang, N.; Zhang, W.-G. *Cryst. Growth Des.* **2012**, *12*, 4441−4449.
(7) Armarego, W. L. F.; Chai, C. L. L. *Purification of Laboratory Chemicals*, 5th ed.; Butterworth-Heinemann: New York, 2003.
(8) Sheldrick, G. M. *SHELXS 97* and *2013 Program for the Solution of Crystal Structures*; University of Göttingen: Göttingen, Germany, 1997 and 2013.
(9) Spek, A. L. *J. Appl. Crystallogr.* **2003**, *36*, 7−13.
(10) (a) Zhang, J.-P.; Huang, X.-C.; Chen, X.-M. *Chem. Soc. Rev.* **2009**, *38*, 2385−2396. (b) Makal, T. A.; Yakovenko, A. A.; Zhou, H.-C. *J. Phys. Chem. Lett.* **2011**, *2*, 1682−1689.
(11) (a) Chang, X.-H.; Ma, L.-F.; Hui, G.; Wang, L.-Y. *Cryst. Growth Des.* **2012**, *12*, 3638−3646. (b) Benelli, C.; Gatteschi, D. *Chem. Rev.* **2002**, *102*, 2369−2387. (c) Moreno Pineda, E.; Tuna, F.; Pritchard, R. G.; Regan, A. C.; Winpenny, R. E. P.; McInnes, E. J. L. *Chem. Commun.* **2013**, *49*, 3522−3524.
(12) (a) Zheng, Y.-Z.; Evangelisti, M.; Tuna, F.; Winpenny, R. E. P. *J. Am. Chem. Soc.* **2011**, *134*, 1057−1065. (b) Li, C.-J.; Lin, Z.-j.; Peng, M.-X.; Leng, J.-D.; Yang, M.-M.; Tong, M.-L. *Chem. Commun.* **2008**, 6348−6350.
(13) Aronica, C.; Chastanet, G.; Pilet, G.; Guennic, B. L.; Robert, V.; Wernsdorfer, W.; Luneau, D. *Inorg. Chem.* **2007**, *46*, 6108−6119.
(14) Actually, the magnetism of **1b** had been reported by: Li.; et al. *Inorg. Chem. Commun.* **2011**, *14*, 522−525. However, our results completely contradict with theirs. We present our results here just for discussion.
(15) (a) Mondal, A.; Durdevic, S.; Chamoreau, L.-M.; Journaux, Y.; Julve, M.; Lisnard, L.; Lescouezec, R. *Chem. Commun.* **2013**, *49*, 1181−1183. (b) Lloret, F.; Julve, M.; Cano, J.; Ruiz-García, R.; Pardo, E. *Inorg. Chim. Acta* **2008**, *361*, 3432−3445. (c) Ma, J.-x.; Huang, X.-f.; Song, X.-q.; Zhou, L.-q.; Liu, W.-s. *Inorg. Chim. Acta* **2009**, *362*, 3274−3278. (d) Sun, H.-L.; Wang, Z.-M.; Gao, S. *Inorg. Chem.* **2005**, *44*, 2169−2176.
(16) (a) Ungur, L.; Thewissen, M.; Costes, J.-P.; Wernsdorfer, W.; Chibotaru, L. F. *Inorg. Chem.* **2013**, *52*, 6328−6337. (b) Towatari, M.; Nishi, K.; Fujinami, T.; Matsumoto, N.; Sunatsuki, Y.; Kojima, M.; Mochida, N.; Ishida, T.; Re, N.; Mrozinski, J. *Inorg. Chem.* **2013**, *52*, 6160−6178. (c) Chandrasekhar, V.; Dey, A.; Das, S.; Rouzières, M.; Clérac, R. *Inorg. Chem.* **2013**, *52*, 2588−2598.
(17) Zou, L.-F.; Zhao, L.; Guo, Y.-N.; Yu, G.-M.; Guo, Y.; Tang, J.; Li, Y.-H. *Chem. Commun.* **2011**, *47*, 8659−8661.
(18) (a) Ma, B.-Q.; Zhang, D.-S.; Gao, S.; Jin, T.-Z.; Yan, c.-H.; Xu, G.-X. *Angew. Chem., Int. Ed.* **2000**, *39*, 3644−3646. (b) Sun, Y.-Q.; Zhang, J.; Chen, Y.-M.; Yang, G.-Y. *Angew. Chem., Int. Ed.* **2005**, *44*, 5814−5817.
(19) Zhao, B.; Cheng, P.; Chen, X.; Cheng, C.; Shi, W.; Liao, D.; Yan, S.; Jiang, Z. *J. Am. Chem. Soc.* **2004**, *126*, 15394−15395.
(20) Rocha, J.; Carlos, L. D.; Paz, F. A. A.; Ananias, D. *Chem. Soc. Rev.* **2011**, *40*, 926−940.
(21) Vicentini, G.; Zinner, L. B.; Zukerman-Schpector, J.; Zinner, K. *Coord. Chem. Rev.* **2000**, *196*, 353−382.